Pulsed thrust measurements using laser interferometry

E. A. Cubbin, J. K. Ziemer, E. Y. Choueiri,[a] and R. G. Jahn
Electric Propulsion and Plasma Dynamics Laboratory, Princeton University, Princeton, New Jersey 08544

(Received 21 October 1996; accepted for publication 20 February 1997)

An optical interferometric proximeter system (IPS) for measuring thrust and impulse bit of pulsed electric thrusters was developed. Unlike existing thrust stands, the IPS-based thrust stand offers the advantage of a *single* system that can yield electromagnetic interference-free, high accuracy ($<2\%$ error) thrust measurements within a very wide range of impulses (100 μN s to above 10 N s) covering the impulse range of all known pulsed plasma thrusters. In addition to pulsed thrusters, the IPS is theoretically shown to be capable of measuring *steady-state* thrust values as low as 20 μN for microthrusters such as the field emission electric propulsion thruster. The IPS-based thrust stand relies on measuring the dynamic response of a swinging arm using a two-sensor laser interferometer with 10 nm position accuracy. The wide application of the thrust stand is demonstrated with thrust measurements of an ablative pulsed plasma thruster and a quasi-steady magnetoplasmadynamic thruster. © *1997 American Institute of Physics.* [S0034-6748(97)00806-X]

I. INTRODUCTION

The performance of many steady-state electric thrusters improves as the operating power level is increased. Due to the limited available power for most foreseeable space missions, instantaneous pulsed high power provides better performance while requiring low average power levels. The ablative pulsed plasma thruster (APPT) and the field emission electric propulsion (FEEP) thruster are currently the only viable high specific impulse propulsion options on small spacecraft with available power levels less than 200 W. These devices are described in Refs. 1 and 2. The mass savings advantage[3,4] pulsed plasma thrusters offer to many near-term power-limited small satellites has renewed interest in these devices and consequently in the accurate measurement of their performance. The most critical performance measurement is that of thrust.

Aside from such microthrusters, there is a need to study the performance of quasi-steady magnetoplasmadynamic thrusters (MPDTs). Quasi-steady MPDTs were originally used in the laboratory as a simulation of steady-state high power thrusters,[5] intended for more futuristic high-power (MW-level) missions.[6,7] With improved energy storage technology quasi-steady MPDTs have since been considered a promising propulsion option. For such thrusters the requirement is not only to measure the total impulse but also to resolve the instantaneous thrust *during* the pulse in order to estimate the equivalent steady-state thrust. This is especially crucial when the current pulse used for steady-state simulation differs from a perfect rectangular pulse. This is often the case when using a real pulse forming network (PFN).[8,9]

Although diagnostic methods already exist for impulse bit and instantaneous thrust measurements of various magnitudes, no *single* high-accuracy diagnostic is known to measure impulse values throughout the entire operating range of typical pulsed plasma thrusters (PPTs) and resolve the thrust of quasi-steady pulsed plasma devices.[10] An optical interferometric proximeter system (IPS) was designed to meet these needs while providing other advantages. While the motivation for this work was measuring the performance of pulsed *plasma* thrusters, the resulting system and methods are applicable for pulsed thrusters in general.

In the past, impulse and instantaneous thrust measurement systems typically used either an inductive proximetry probe,[11,12] an accelerometer,[8,9] a linear voltage differential transformer (LVDT),[13,14] a differential plate capacitance system,[15] or an optical angular readout.[16] The most sensitive of these past devices appears to be the optical angular readout from Ref. 16, designed in 1968 at NASA Jet Propulsion Laboratory (JPL), which can measure thrust as low as 5 μN with loads up to 12 kg. A comparable thrust stand was designed at Goddard Space Flight Center in 1970 that measured thrust as low as 25 μN, thrust stand deflection as low as 25 nm, and measured the thrust vector.[15] Larger thrust and impulse bit measurements have been made as well. A 5 N thrust stand was developed by Haag[17] at NASA Lewis Research Center in 1989 and impulse bits near 1 N s were measured at Princeton University.[5,8]

The IPS thrust stand was designed to accurately measure ($<2\%$ error) impulse bits for all practical pulsed plasma thrusters within the range of 100 μN–10 N s. It is also capable of measuring low steady state thrust down to below 20 μN. This article addresses thruster performance measurement fundamentals. The IPS design and operation is fully described. Experimental results obtained with the IPS-based thrust stand and a full error analysis are presented.

II. THRUST MEASUREMENT FUNDAMENTALS

A. Thrust and impulse bit

Performance measurements for a given thruster will rely on one of two different values: the total delivered impulse or the instantaneous thrust. Both are done by analyzing the thrust stand dynamics. A swinging arm type thrust stand is used in our experiments and is described in Sec. III. Impulse bit measurements require measuring the thrust stand dynam-

[a]Electronic mail: choueiri@princeton.edu

ics before and after the delivered impulse. Instantaneous thrust measurement requires measurements during the thrust.

B. Thrust stand dynamics

Thrust stand systems can be treated like a ''black box.'' The input to the system is the applied thrust and the response of the system can be observed from many locations within the thrust stand system. The exact dynamic response of each observation point on a thrust stand to a given thrust input can, in general, be complicated. Fortunately, in many cases the thrust stand can be modeled with a high degree of accuracy as a damped spring-mass system. If the motion of the observation point is characterized by x, and the effective natural frequency, damping constant, and mass are $\omega_{n,\mathrm{eff}}$, ζ_{eff}, and m_{eff}, respectively, the applied impulse bit (I_{bit}) will force the response[18]

$$x(t)=e^{-\zeta_{\mathrm{eff}}\omega_{n,\mathrm{eff}}\,t}\frac{I_{\mathrm{bit}}/m_{\mathrm{eff}}}{\omega_{n,\mathrm{eff}}\sqrt{1-\zeta^2}}\sin(\sqrt{1-\zeta^2}\,\omega_{n,\mathrm{eff}}t). \quad (1)$$

The duration of the impulse must be much less than the natural period of the observation point for Eq. (1) to be valid. In many such cases, measurements can be made on timescales where the effects of the spring and damper are negligible. In the absence of a spring and damper, this model leads to the simple momentum equation,

$$I_{\mathrm{bit}}=m_{\mathrm{eff}}\Delta\dot{x}, \quad (2)$$

where $\Delta\dot{x}$ is the change in velocity of the observation point from before to after the impulse. Likewise, for a free body, Newton's equation,

$$\ddot{x}=T/m_{\mathrm{eff}}, \quad (3)$$

governs the dynamics where $\ddot{x}$ is the acceleration of the observation point and T is the instantaneous thrust. In order to compute I_{bit} or T, a calibration constant, the effective mass (m_{eff}), for the thrust stand must be determined. This can be done by applying a known impulse to the system and observing the dynamic response. This is discussed in Sec. II D. Whether the appropriate model is this simple or not, the position coordinate provides the dynamic response of the system to an excitation. The IPS was designed around this idea and can accurately provide continuous position data with a maximum resolution as high as 10 nm.

C. Position measurement with the IPS

The IPS is based on the Michelson interferometer.[19] The optical nature of this system is one essential feature that solves the electromagnetic interference (EMI) problem common to high current PPTs. Another essential feature is the high spatial resolution capability of optical interferometry.

Figure 1 shows a schematic of the IPS. Light emitted from the laser source is split into two beams at the beam splitter. At the end of each path is a corner cube. The two beams are reflected back to the beam splitter and passed through a lens to the diode sensors. The diode sensor output signals are recorded on a computer. Multiple fringes are facilitated by slightly offsetting the two beams at the diode

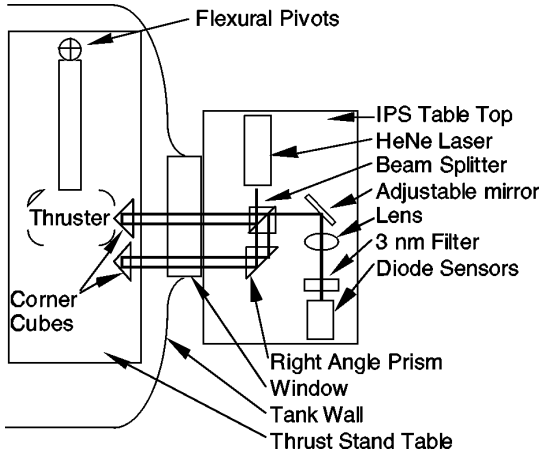

FIG. 1. IPS layout.

sensors. When the path lengths traversed by the two beams differ by a non-integer multiple of the wavelength of the laser light (λ) there is a phase angle difference (ϕ) between them when they are reunited. Superposition of these two waves yields constructive or destructive interference. If only one corner cube is allowed to move, then it can be shown that the intensity of light (I) at a particular location on the diode array is related to the relative position (x) of the corner cube by[20]

$$I(t)=\frac{I_{\max}}{2}\left[1+\cos\left(\frac{4\pi x(t)}{\lambda}\right)\right]. \quad (4)$$

Equation (4) shows that, if $\dot{x}$ is constant, $I(t)$ will appear as a continuous cosine function with a constant frequency (ω_{IPS}) of

$$\omega_{\mathrm{IPS}}=\frac{4\pi\dot{x}}{\lambda}. \quad (5)$$

The frequency of the IPS output signal increases with the velocity of the observation point. Relative motion of two locations on the thrust stand can also be measured to ''scale down'' larger motions if desired. In either case, the dynamic motion of the thrust stand can be observed via the fringe pattern.

There are two disadvantages to using a single diode sensor to monitor the fringe pattern. From Eq. (4), the position can be obtained by properly taking the arccosine of the intensity signal. The first disadvantage of this technique is that the sensitivity of the cosine function goes to zero at maximum and minimum light intensities. In other words [again consider Eq. (4)] if the intensity is at maximum when a change in x occurs, the result is a relatively small change in the light intensity. Compare this to the case when the present light intensity level is between a maximum and a minimum in which case the resulting change of light intensity is much larger and quite linear.

A second disadvantage to using a single diode sensor to monitor position is that direction reversals can sometimes go undetected. When x is a half-integer multiple of λ, I is at a maximum. No matter which way x moves from this point in

time, the intensity will diminish, thus direction ambiguity can occur. Both of these disadvantages can be eliminated by using a double diode sensor.

In order to use the double diode sensor, the interference pattern at the diode sensors should not be uniform. This can be achieved by several different methods. For example, offsetting the two interfering beams before they reach an expanding lens will result in fringes similar to those in Younge's double-slit experiment.[19] In this case, as x changes, two given locations within the fringe pattern will change intensity with frequency ω_{IPS} but these resultant cosine curves will be out of phase. By selecting two points within the fringe pattern that are 90° out of phase, there is always one diode sensor output signal in the sensitive region of the cosine function. One way to unfold this double sensor information is to use a scheme called continuous quadrature. Normalizing the two outputs and plotting one signal versus the other will produce data which fall on the unit circle. In this case the angle is proportional to x. An algorithm can be written which properly takes the arctangent of the data and gives the position versus time. One cycle around the unit circle corresponds to a distance $\lambda/2$. The algorithm must be able to handle many cycles around the circle as well as direction reversals. The spatial resolution obtained for these experiments was 10 nm and is described in Sec. V A. This technique was used in several experiments and the results are in Secs. IV A and IV B.

D. Calibration of the IPS based thrust stand

Once two locations are chosen for the relative x measurement, the effective mass (m_{eff}) must be determined. This process is synonymous with calibrating the IPS-based thrust stand. A known impulse must be given to the thrust stand while the response is recorded by the IPS. The impulse must be applied at the same location as the force which is applied during an actual firing of the thruster. A commercially available force transducer provides a simple way of applying a measurable impulse. The thruster must be struck with the force transducer while the force transducer output voltage is being recorded. Integrating the force with respect to time yields total impulse. The IPS should record the response of the thrust stand to the impulse. From the measured change in velocity (Δv), m_{eff} can be determined using the measured total impulse for I_{bit}:

$$m_{\mathrm{eff}}=\frac{I_{\mathrm{bit}}}{\Delta v}. \tag{6}$$

III. EXPERIMENTAL SETUP

A. Vacuum facilities

The vacuum vessel is a 2-m-diam, 5-m-long fiberglass tank with eight optical access ports. A vacuum level on the order of 10^{-5} Torr is maintained by a set of two 1.3 m diffusion pumps each with a pumping capacity of 95 m^3/s. The diffusion pumps are backed by a Roots blower (1340 cfm) and two mechanical pumps (150 cfm).

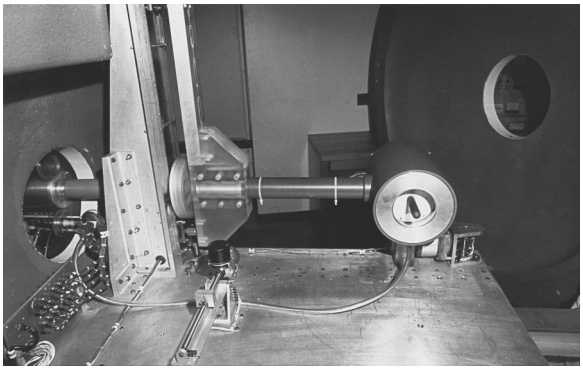

FIG. 2. Quasi-steady MPDT and thrust stand.

B. Power supply

The power supply consists of a 20-station 12.8 mF L-C PFN that can be adjusted to produce current pulses ranging from 0.5 to 2 ms at current levels up to 50 kA. This power supply is used for the quasi-steady MPDT discussed in Sec. IV C. The APPT discussed in Sec. IV A has internal energy storage and pulsing subsystems and requires an external 15–30 V unregulated 30 W power supply.

C. Thrust stand arm

The thruster is mounted on a swinging arm thrust stand. Figure 2 shows a gas-fed coaxial MPDT attached to the arm. The thrust arm is mounted with two flexural pivots. They are series 6016 Bendix free-flex pivots[21] each with a torsional spring constant of 0.73 N m/rad. The vertical axis of rotation of the arm can be adjusted to incorporate the force of gravity. The force of gravity can be added or subtracted from the restoring force of the flexural pivots to influence the natural period of the arm. Typical natural periods of the arm are 1–10 s. The thrust stand arm is fully described in Ref. 5 and is a modified version of a microthrust stand built by Fairchild Republic.[13] To reduce random mechanical perturbations to the thrust stand system, the entire thrust stand table was mechanically isolated from the tank. This was done by resting the entire structure on rubber supports.

D. IPS assembly

At the thruster end of the tank the IPS table top was mounted at the optical access window. Figure 1 is a layout of the IPS. One corner cube is attached to the thrust stand table and the other to the thruster. A 1 mW helium-neon laser ($\lambda=632.8$ nm) was used as a light source in the interferometer. Both the beam splitter and the right angle prism were mounted on two adjoined aluminum blocks with separate pitch angle adjustment. Also, the beam splitter and right angle prism can each slide sideways to match the horizontal separation of the corner cubes. Both of these adjustments are made until both beams are nearly coincident at the adjustable mirror. The mirror is then used to direct the beams to the diode sensors. Between the mirror and the diodes are a lens and a filter. The lens is a cylindrical lens of focal length 1 cm. Finally there is a 3 nm bandwidth filter at wavelength 632.8 nm. This prevents virtually all stray light from the

surrounding area from reaching the diode sensors, including light from the plasma discharge. The diode sensors are FDS100 silicon photodiodes from Thorlabs Inc. They have a rise time of 10 ns, an active area of 13.7 mm^2, and a spectral response of 350–1100 nm.

E. Calibration pendulum

The calibration impulse was delivered by a 30-cm-long 0.5-kg-steel rod that was used as a pendulum. The rod pivots on a Teflon pin that was fixed to an aluminum stand. This stand was mounted inside of the vacuum tank in front of the thruster and struck the thruster while the vacuum tank was exposed to atmosphere. An electromagnet was also mounted on the pendulum stand so that the pendulum could be cocked and then released remotely. Care must be taken to align the pendulum so that the force is delivered along the thrust axis. A quantification of this alignment error will be discussed in Sec. V B.

The force transducer used was a model 208A02 force transducer from Piezotronics that was attached to the end of the pendulum and struck the thruster. The operating range is from 0 to 400 N. The output signal during an impact is recorded on a Nicolet 320 Digital oscilloscope and then analyzed on a computer. The data was digitally integrated to obtain a value for I_{bit}. For a discussion of the force transducer calibration and integration error, see Sec. V B.

IV. EXPERIMENTAL RESULTS

A. Impulse bit measurement of the APPT

The APPT used for this experiment is the Lincoln Experimental Satellite thruster (LES-8/9).[2] The APPT has a mass of 6.6 kg and has a total impulse capability of 7320 N s. The impulse bit is nominally 300 μN s and the specific impulse is 1000 s. The PFN is internal and requires an external 25–150 W power supply to charge the main 17 μF oil-filled capacitor. The pulse lasts for 5–10 μs and can pulse at a maximum of 2 Hz. The discharge occurs across the surface of a Teflon fuel bar and ablates approximately 30 μg of propellant. There are two nozzles canted 30 degrees to the thruster axis of symmetry. For these experiments only one nozzle was fired. The APPT was mounted on the thrust stand such that the nozzle was perpendicular to the thrust arm.

On short time scales, the free-mass model for impulse bit calculations is always valid. However, it may be that the background noise disallows accurate $\dot{x}$ measurements to be made. In this case, a second alternative is to observe longer timescales and model the system with more complexity. In the case of a damped spring-mass system, Eq. (1) describes the dynamic response. Using the force transducer method described in Sec. II D and demonstrated in Sec. IV C the effective mass was determined. An insert was made to fit into the nozzle. The calibration pendulum struck the center of the insert. The result was $m_{\text{eff}}=12.16\pm0.21$ kg. The IPS configuration for the APPT experiments was also as shown in Fig. 1. For small damping, the maximum displacement (Δx) for this system is

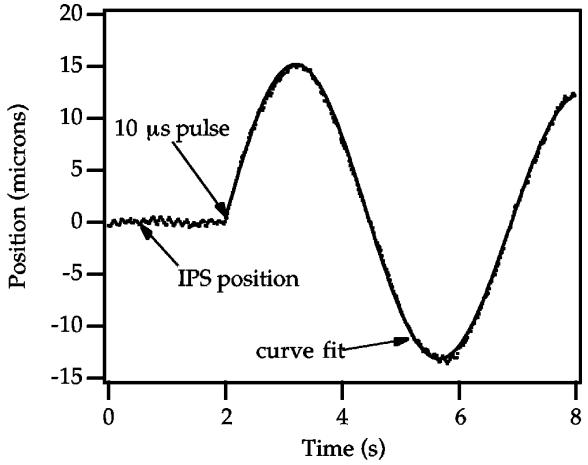

FIG. 3. IPS position data with curve fit.

$$\Delta x=\frac{2I_{\text{bit}}}{\omega_{n,\text{eff}}\, m_{\text{eff}}}. \tag{7}$$

Therefore, restoring forces on the thrust arm were minimized such that $\omega_{n,\text{eff}}$ was minimized and the resultant signal-to-noise ratio for position was 60:1 at maximum deflection. Section V discusses this quantitatively. Once the effective mass is known, the position data from a damped spring-mass system can be fit to the model unambiguously. Equation (1) requires ζ_{eff}, $\omega_{n,\text{eff}}$, and I_{bit} for a fit. Figure 3 shows the raw, unfolded double IPS sensor position data and the curve fit. The corresponding fit values are $\zeta_{\text{eff}}=0.0326$, $\omega_{n,\text{eff}}=1.279$ rad/s, and $I_{\text{bit}}=0.285$ mN s. The uncertainty on I_{bit} was found to be ±0.005 mN s (1.75%).

B. Steady-state microthrust measurement

Recent interest in microthrusters ($T<1$ mN) is accompanied by the desire to accurately measure its performance capabilities. FEEP thrusters, for example, are typically designed in the 10–100 μN thrust range.[22] As described in Sec. V C, the low frequency operation of the IPS can detect motion in the micron regime. In Sec. IV A this is demonstrated with the LES 8/9 APPT. Assuming the thruster and mounting hardware mass are less than 25 kg, a 100 μN thrust left on for 1 s will cause a displacement of approximately 15 μm. This can easily be detected by the IPS and allows a thrust measurement to be made.

Smaller thrust levels can be accommodated as well. As the thrust level drops, the thruster must be left on for a longer time to produce a measurable displacement of the thrust arm. As this time becomes comparable to the natural period of the thruster arm, the damped sinusoidal model [Eq. (1)] becomes inappropriate. In this case, a steady-state displacement method can be used. The effective spring constant on the thrust arm (k_{eff}) is easily determined from the information in Sec. IV A as

$$k_{\text{eff}}=m_{\text{eff}}\omega^2\approx 20\ \ \mu\text{N}/\mu\text{m}. \tag{8}$$

This indicates that a 20 μN thruster will produce a steady state displacement of the thrust arm of 1 μm, a distance

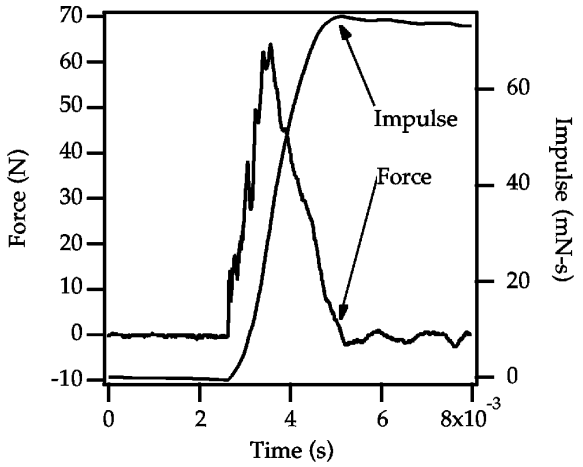

FIG. 4. Force delivered by the pendulum and the integrated force for total impulse.

within the measuring capability of the IPS. By carefully aligning the thruster arm to a nearly horizontal position, the effects of gravity, which contribute to k_{eff}, were further reduced to yield a $k_{\text{eff}} \approx 10\ \mu\text{N}/\mu\text{m}$. It is therefore estimated that the IPS can measure microthrust levels as low as 10 μN, a range that includes most FEEP thrusters. The precise accuracy of such a measurement with the IPS would have to be experimentally determined.

C. Impulse bit and thrust of a quasi-steady MPDT

1. The quasi-steady MPDT

The benchmark configuration[5] of a coaxial quasi-steady MPDT has a 12.7-cm-diam anode with a 10-cm-long hemispherically tipped, 1.9-cm-diameter cathode, a 5-cm-deep chamber and an anode inner radius of 5.1 cm. Propellant injection is at the back plate of the chamber. Argon at 6 g/s was used. A 15 ms flat-top current pulse of approximately 15 kA is applied and the self-induced magnetic field accelerates the plasma out of the discharge chamber. The operating voltage is a nominal 100 V.

The most convenient model of the thrust stand system to use with the quasi-steady MPDT is the free-mass model. In this case Eq. (2) is employed and only m_{eff} needs to be determined.

The IPS was configured as shown in Fig. 1. The pendulum stand (see Sec. II D for details) was placed in front of the MPDT so that the force transducer would strike the tip of the cathode. Figure 4 shows the measured force and the calculated total impulse. The double sensor IPS response to the impact test is shown in Fig. 5. This sensor data were unfolded to produce position information, shown in Fig. 6. The natural period of the thrust stand was approximately 1 s. Therefore on timescales much shorter than 1 s, the effects of the effective spring and damping are negligible. In this case m_{eff} is found from Eq. (2), the impulse delivered was 75.1 mN s and thus

$$m_{\text{eff}} = \frac{I_{\text{bit}}}{\Delta \dot{x}} = \frac{75.1\ \text{mN s}}{4.78\ \text{mm/s}} = 15.71 \pm 0.27\ \text{kg}. \tag{9}$$

2. Impulse bit

With the IPS calibrated for this thrust stand arrangement, the quasi-steady MPDT was fired and the IPS response was once again recorded. A slope change of 5.79 mm/s was recorded. From Eq. (2) and m_{eff}, the delivered impulse is

$$I_{\text{bit}} = 15.71\ \text{kg} \times 5.79\ \text{mm/s} = 0.091 \pm 0.0016\ \text{N s}. \tag{10}$$

3. Instantaneous thrust

Time resolved position data are also of interest with the quasi-steady MPDT. Equation (3) shows that if the free-mass model is accurate, only $\ddot{x}$ is needed for determining instantaneous thrust. The IPS proved immune to EMI and is shown in Fig. 7. The IPS successfully recorded the dynamic response of the MPDT during the current pulse.

Position (x) is differentiated twice and is shown in Fig. 8. The acceleration error is 2% and is discussed in Sec. V D *3*. The $\ddot{x}$ data reveal information about the validity of

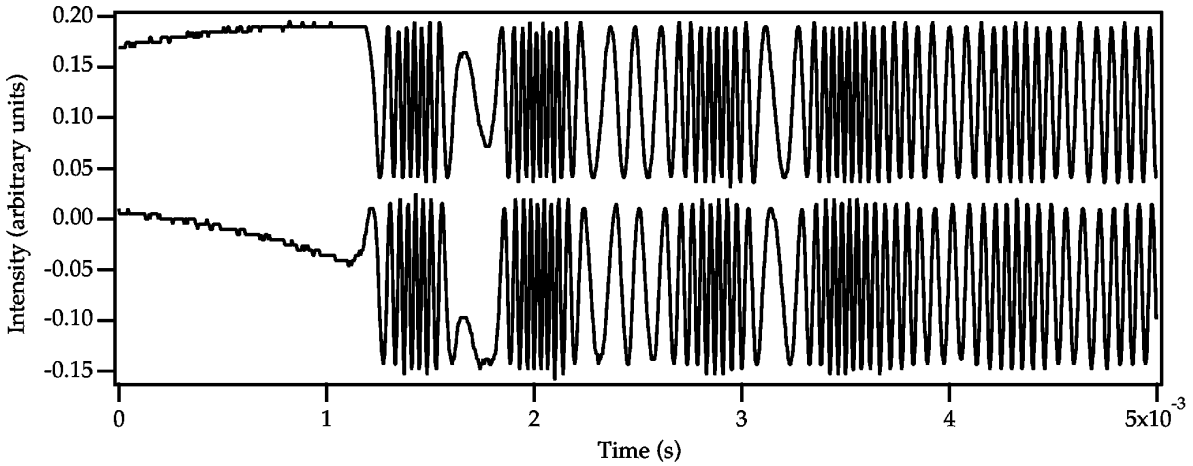

FIG. 5. IPS output during pendulum impact.

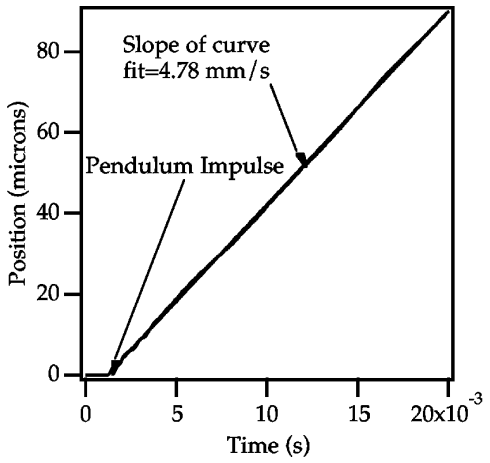

FIG. 6. IPS position measurement after pendulum impact.

the free-mass model. The actual acceleration of the thruster fluctuates. This is typically due to structural vibrations within the thruster. Vibration observed before the current pulse (see Fig. 8) is caused by opening of the solenoid valve presently located on the thruster. Solutions to this problem include stiffening the thruster and the thrust arm. The goal of this experiment was to demonstrate the capability of the IPS to resolve *acceleration*. Stiffening of the thruster has been accomplished in the past[8,9] and must be done before any attempt to extract resolved thrust information from the recorded acceleration.

V. ERROR ANALYSIS

An error analysis for the different IPS measurements is now discussed. First the IPS raw measurement error of 10 nm is experimentally determined. Then the background mechanical perturbations to the system are considered in an error analysis of the impulse bits reported above. Each final impulse value was comprised of a m_{eff} measurement and a value from a curve fit. The m_{eff} error will be determined from the accuracy of the force transducer and the estimated experimental error of alignment, and the error associated with the curve fit values will be estimated from a statistical approach, again considering the background mechanical noise.

A. IPS position error

The IPS position error is established by aiming both beams of the interferometer into the same corner cube. This conservatively reveals the internal noise of the IPS. Figure 9 shows 1 s of noise. The standard deviation on this noise is 10 nm.

B. Error in m_{eff} measurement

The calibration constant for the force transducer was determined by applying 30 different vertical static loads over the range of 0–100 N. A line was fit to the data and the resultant calibration constant was found to be 87.6 ± 0.6 N/V. The integration was done numerically on a computer. The zero level was taken as the average value for 1 ms before the impact (see Fig. 4). This value varied much less than 1% of the peak signal strength so it was negligible. Integration can be done to an accuracy of 1%.

A last source of error is the alignment of the calibrating pendulum with the thrust axis. If an alignment of 3° is maintained, the error incurred is 0.1%. The pendulum was aligned to this tolerance so the incurred error was negligible. Summing the errors identified in this section yields a 1.7% error for the m_{eff} measurement. This measurement was done five times whenever a new thruster was mounted on the thrust stand or when the thruster was modified and was always repeatable to within the accuracy of integration.

C. IPS signal-to-noise ratio: Choosing a technique

The IPS is capable of measuring position data in many frequency and amplitude regimes. Since the IPS can be used in different ways to measure the same thruster performance

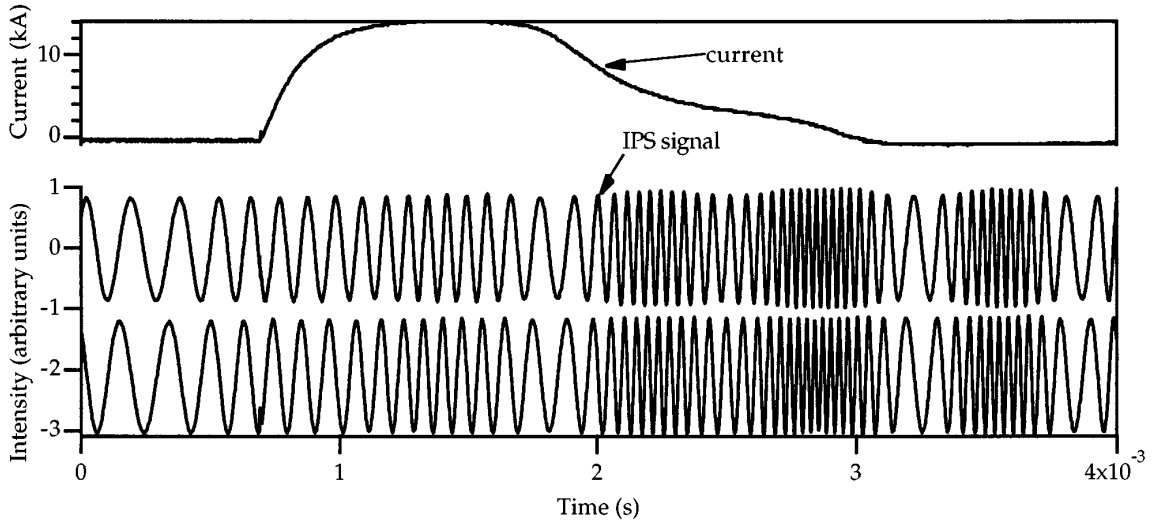

FIG. 7. IPS output during a quasi-steady MPDT pulse.

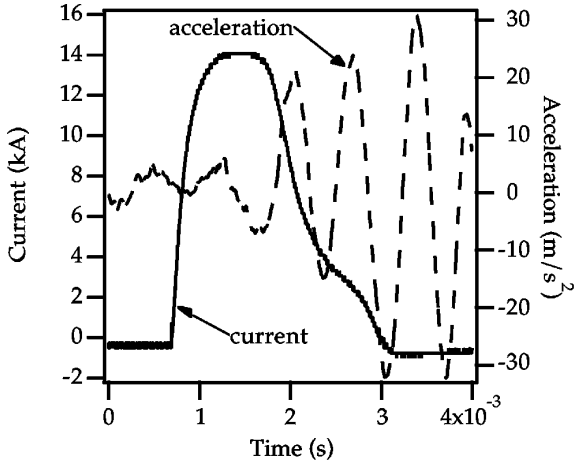

FIG. 8. IPS acceleration during an MPDT pulse.

value (i.e., Δv measurement, steady-state displacement measurement, or damped sinusoidal fit), it is necessary to find a way of choosing the best technique. This can be done by considering the power spectrum of the background noise.

The power spectrum of the background noise indicates which of the various measurement techniques should be used to obtain a thrust measurement. One must first calculate what ideal response of the thruster arm is expected from the predicted impulse. For instance, for the sinusoidal response, the strength of the signal expected (as in Fig. 3) can be compared to the background noise at the natural frequency of the arm. This will give a signal-to-noise value and indicates the accuracy of the IPS for this type of measurement. If needed, a band-pass filter can be applied to the raw IPS data to eliminate background noise before the curve fitting process is begun. Each technique should be considered and the one with the highest signal-to-noise ratio will provide the most accurate measurement.

D. Curve fitting the data

1. A linear fit

All of the curve fit data were performed using the software package IGOR PRO by WaveMetrics. In the case of the quasi-steady MPDT I_{bit} calculation, $\dot{x}$ was found using a line fit to the position data after the pulse. If the scatter of the data around the fit is considered to be noise, a standard deviation value can be computed for the slope. This computed value was 0.1% of the slope.

2. A damped sinusoidal fit

Fitting Eq. (1) to the IPS position data yields a 0.1% standard deviation in the estimate of $\dot{x}(0)$ for the APPT. The present curve fitting method uses all of the position data 0.5 s prior to the pulse to obtain a small initial velocity value which is typically $<1\%$ of $\dot{x}(0)$ and is appropriately added or subtracted from $\dot{x}(0)$. Combining the 0.1% standard deviation with the 1.7% error of the effective mass error yields approximately 1.8% error on the APPT impulse.

3. Time resolved acceleration

The position information obtained during the pulse of a thruster can be differentiated twice for actual acceleration information. It is necessary to first quantify the background noise in this acceleration measurement. Figure 10 contains a sample of the background position data taken when the MPDT is not firing. By differentiating this data twice, the background acceleration can be quantified. Figure 10 shows the results. The maximum background acceleration appears to be 0.06 m/s^2 and is always repeatable. The steady-state thrust for the benchmark MPDT should produce an acceleration of approximately 3 m/s^2.[8] The background noise is thus 2%.

VI. DISCUSSION

The IPS has demonstrated the ability to accurately measure ($<2\%$ error) pulsed thruster performance for thrusters in the range of 1×10^{-4} N s and 0.1 N s nominal impulse values with an immunity to electromagnetic interference that is common to pulsed electric thrusters. For our particular devices we measured an impulse bit for the ablative pulsed plasma thruster of 0.285 ± 0.005 mN s and a quasi-steady MPDT impulse bit of 0.091 ± 0.0016 N s. Instantaneous ac-

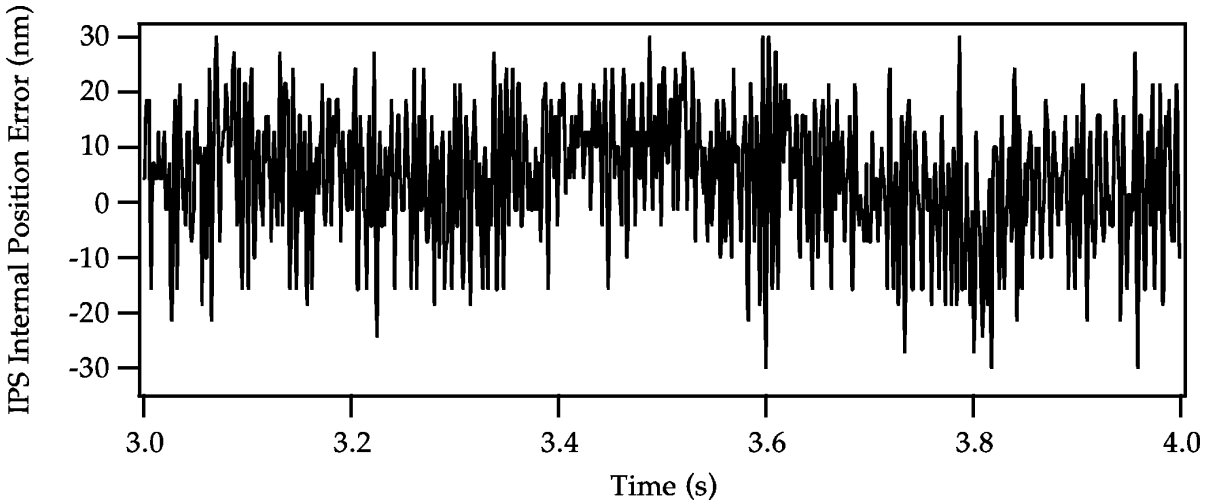

FIG. 9. IPS internal noise position data.

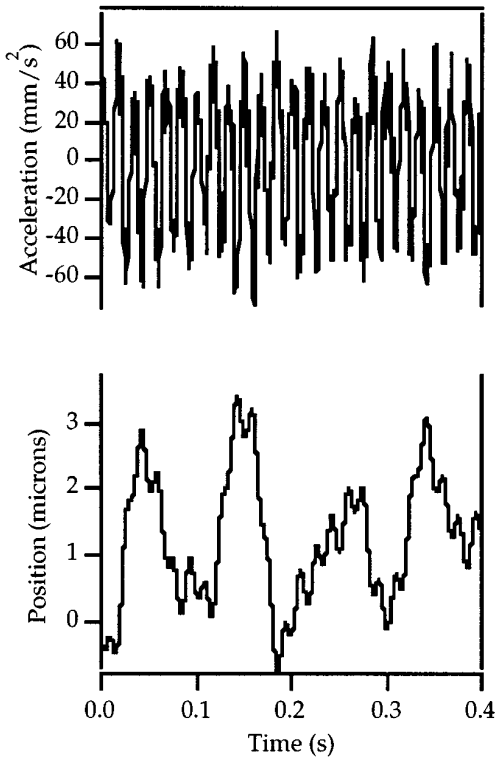

FIG. 10. Background noise measured by IPS for quasi-steady MPDT configuration.

celeration measurements can be made with a sufficiently stiffened MPDT in the 100 N range with an error of $<2\%$. We also have shown that the IPS can measure thrust levels down to 20 μN, a range that includes most microthrusters such as those of field emission electric propulsion.

[1] S. Marcuccio, A. Ciucci, H. Oest, A. Genovese, and M. Adrenucci, 32nd Joint Propulsion Conference, Lake Buena Vista, FL, 1–3 July 1996.
[2] R. J. Vondra and K. I. Thomassen, J. Spacecr. Rockets **11**, 613 (1974).
[3] R. M. Myers and S. R. Oleson, 29th Intersociety Energy Conversion Engineering Conference, Monterey, CA, 7–11 August 1994.
[4] E. Y. Choueiri, J. Spacecr. Rockets **33**, 96 (1996).
[5] R. L. Burton, K. E. Clark, and R. G. Jahn, J. Spacecr. Rockets **20**, 299 (1983).
[6] K. Kuriki, K. Toki, and Y. Shimizu, Technical Report No. EXP-R-i003-0, Institute of Space and Astronautical Science, Tokyo, Japan, 1987.
[7] E. Y. Choueiri, A. J. Kelly, and R. G. Jahn, J. Spacecr. Rockets **30**, 749 (1993).
[8] J. M. Berg, A. J. Kelly, and R. G. Jahn, 17th International Electric Propulsion Conference, Tokyo, 27–29 June 1984.
[9] K. Kuriki and H. Suzuki, 12th International Electric Propulsion Conference, Key Biscayne, FL, 14–17 November 1976.
[10] E. A. Cubbin, J. K. Ziemer, E. Y. Choueiri, and R. G. Jahn, 24th International Electric Propulsion Conference, Moscow, Russia, September 1995.
[11] Progress Report No. EPPDyL-TR-94F, Princeton University, June–December 1994.
[12] Technical Report No. L5001, Bently Nevada Corporation, April 1990.
[13] Technical Report No. RAC 2392-1, PCD-TR-65-1, Republic Aviation Corporation, January 1965.
[14] T. W. Haag, 31st Joint Propulsion Conference and Exhibit, San Diego, CA, July 1995.
[15] Technical Report No. NASA TN D-7029, August 1971.
[16] A. V. LaRocca and P. Malherbe, 4th Propulsion Joint Specialist Conference, Cleveland, OH, 10–14 June 1968.
[17] T. W. Haag, Rev. Sci. Instrum. **62**, 1186 (1991).
[18] W. T. Thomson, *Theory of Vibrations With Applications* (Prentice-Hall, Englewood Cliffs, NJ, 1993).
[19] G. R. Fowles, *Introduction to Modern Optics* (Dover, New York, 1989).
[20] R. A. Serway, *Physics for Scientists and Engineers* (Saunders College, Chicago, 1990).
[21] Technical Report No. 00U-6-681D, The Bendix Corporation, Fluid Power Division, March 1972.
[22] M. Andrenucci, in Ref. 10.